

First-principle calculation of the dielectric and dynamical properties of orthorhombic CaMnO_3

Satadeep Bhattacharjee, Eric Bousquet and Philippe Ghosez

Physique Théorique des Matériaux, Université de Liège

Abstract

The electronic structure and lattice dynamics of bulk CaMnO_3 is computed in its orthorhombic structure from the first principle using the density functional approach in the framework of local spin density functional theory. The lattice dynamics is performed using density functional perturbation theory (DFPT). The obtained the ground state structural parameters and positions are in good agreement with the experiment. Both IR active and Raman active modes are discussed. We observe that the dynamical charges are anomalously large. The static dielectric constant is large and highly anisotropic.

I. INTRODUCTION

Magnetic perovskite oxides constitute a subject of study because of their wide variety of interesting properties. The interplay between structural, magnetic and transport properties in these systems make them fascinating from both experimental and theoretical point of view. For example, the mixed valent perovskite $Ca_{1-x}La_xMnO_3$ is one of the most studied material for its colossal magnetoresistance (CMR) properties[1] The oxygen deficient manganites $LaMnO_{3-\delta}$ or $CaMnO_{3-\delta}$ are interesting for their transport and optical properties[2]. In this paper we report study on stoichiometric $CaMnO_3$. The crystal structure of $CaMnO_3$ is orthorhombic with space group Pnma[3]. The structure could be regarded as distorted perovskite structure having four formula per unit[3, 4]. The neutral ionic configuration of $CaMnO_3$ is $(Ca^{+2}Mn^{+4}O^{-2})$. Because of Mn^{+4} configuration, the Mn atom is a bad Jahn-Teller ion and the Jahn-Teller distortion is usually negligible. The magnetic structure is antiferromagnetic and $G - type$ antiferromagnetic order is energetically most favourable. The magnetic interaction between the Mn ions are due to superexchange interaction. The observed Neel temperature is about 130 K, which estimates the exchange energy to be 6.6 meV. It is an insulator with observed band gap of about 3eV[5].

Most of the previous first principle calculation on $CaMnO_3$ both in cubic as well as orthorhombic phase focuss mainly on the electronic structure of the system. It is interesting to study the dielectric and vibrational properties from the first principle. In this paper we report results for our calculation of the zone center phonons and dielectric properties from the first principle in the orthorhombic phase of bulk $CaMnO_3$.

II. TECHNICAL DETAILS

The first-principles simulations were made according to the density functional theory scheme (DFT) with the local density approximation (LDA) through the plane-wave implementation of the ABINIT package [8]. We used the Hartwigsen-Goedecker-Hutter [10] (HGH) parametrization for the pseudopotentials, where the 3s and 3p orbitals were treated as valence for Mn and Ca atoms and 2s and 2p orbitals were considered as valence for O atoms. The total number of valence electron was 15 for Mn, 10 for Ca and 6 for oxygen. Convergency was reached with an energy cutt-off of 72 Hartree for the plane wave

expansion and a grid of $6 \times 4 \times 6$ k mesh. The phonons frequencies, Born effective charges (BECT) were computed according to the density functional perturbation theory [9] (DFPT) as implemented in the ABINIT package.

III. RESULTS AND DISCUSSION

A. Structure

At high temperature, CaMnO_3 adopts cubic perovskite structure. At room temperature, the stoichiometric CaMnO_3 is antiferromagnetic and crystalizes in an orthorhombic $Pnma$ (N.62) structure with 20 atoms in the primitive cell [3]. This orthorhombic phase results from the relaxation of three kinds of antiferrodistortive (AFD) instabilities which are related to rotations of oxygen octahedras around the Mn-O axis. In Glazer's notation, these tilts are described by $a^-b^+c^-$. In this orthorhombic structure, CaMnO_3 could be descibed as a pseudocubic compound, since the structural distortions do not affect strongly the equivalent high symmetric structure and the volume could be calculated as $\sqrt{2}a_c \times 2a_c \times \sqrt{2}a_c$ where a_c is the pseudocubic cell parameter.

In our calculations we did the structural relaxation at fixed volume. The volume used corresponds a pseudocubic cell parameter of 3.73\AA which agrees with the experimental high temperature cubic structure. The cell shape and atomic positions are relaxed according to this constrain and the results obtained are reported in TAB.I. The calculated structure is in a good agreement with the experimental datas. The cell parameter a is slightly larger than the pseudocubic structure for both, experimental and calculated structures, while the parameter c is slightly underestimated in both cases compared to that of pseudocubic structure. However the b distance is calculated as being bigger than the ideal cubic structure instead of smaller for experimental results. The calculated atomic positions are also in good agreement with the experimental results. The deviation with the ideal cubic positions are the same for all atoms and for both, calculation and experiment. The amplitude of this deviation is well calculated for oxygens atoms with an average error of about 5%, however this error is bigger for the deviation of Ca atom, since an average error of about 27% is observed on the atomic position. In summary, the calculated structure at fixed volume is in good agreement with respect to the reported experimental results.

	This work	Exp.[3]	pseudocubic
a	5.287	5.279	5.275
b	7.498	7.448	7.46
c	5.235	5.264	5.275
a_c	3.730	3.726	
Ca (4c)			
x	0.040	0.033	0.0
y	0.25	0.25	0.25
z	-0.008	-0.006	0.0
Mn (4b)			
x	0.0	0.0	0.0
y	0.0	0.0	0.0
z	0.5	0.5	0.5
O ₁ (4c)			
x	0.485	0.490	0.5
y	0.25	0.25	0.25
z	0.071	0.066	0.0
O ₂ (8d)			
x	0.287	0.287	0.25
y	0.036	0.034	0.0
z	-0.288	-0.288	0.25

TABLE I: Calculated and experimental cell parameters (\AA) and non-equivalent atomic positions (reduced coordinates) of orthorhombic $Pnma$ CaMnO_3 . Commas relate the Wyckoff site of the reported atoms. The third column relate the equivalent pseudocubic ideal perovskite structure with $a_c=3.730\text{\AA}$ for the calculated structure and 3.726\AA for the experimental datas.

B. electronic properties

From the calculated electronical density of states (DOS), we obtained a band gap of 0.8 eV. This band gap is strongly underestimated with respect to its experimental value (3.1 eV [15]) but this is related to the LDA approximation which gives systematic underestimated

band gap of insulator compounds. The projected DOS on Mn and O atoms (Fig.1) show an origin of electronic band gap from the d orbitals of Mn atoms. This is in agreement with previous calculation on the cubic phase[17], but in contradiction with experimental prediction on the orthorhombic phase where the band gap is expected to be between the O 2p and Mn d orbitals[5].

In TAB.II we report the Born effective charge tensors (BECT) of the four inequivalent atoms of TAB.I. The nominal ionic charges of Ca, Mn and O atoms are respectively 2, 4 and -2. The amplitude of calculated Born effective charges are higher than their nominal values and off-diagonal terms appear for all atoms. The BECT of Mn and O₂ has strong off-diagonal terms. These off-diagonal terms are related to the distortions of the orthorhombic structure with respect to the cubic reference, since the rotations of oxygens change the Mn-O interactions from isotropic, in the ideal cubic perovskite, to asymmetric environment in the orthorhombic structure. These strong off-diagonal terms are unexpected since the deviations from the ideal cubic structure are relatively small, but this behaviour was also reported for CaTiO₃. The eigenvalues of the symmetric part of BECT are also reported in TAB.II. These eigenvalues are relatively anomalous with respect to their nominal charges, mainly for Mn and O atoms. Anomalously high BECT is a general characteristic in ABO₃ perovskites [13], mainly for B and O atom, which is related to a strong charge transfer between these two atoms due to hybridization between B and O valence orbitals.

$$\begin{array}{cc}
 \text{Mn} & \begin{pmatrix} 6.82 & -0.37 & -0.72 \\ 0.07 & 5.78 & 1.42 \\ -0.69 & -1.54 & 6.56 \end{pmatrix} & \text{Ca} & \begin{pmatrix} 2.51 & 0.00 & 0.19 \\ 0.00 & 2.43 & 0.00 \\ 0.27 & 0.00 & 2.52 \end{pmatrix} \\
 & [7.41 & 6.05 & 5.70] & & [2.29 & 2.74 & 2.43] \\
 \\
 \text{O}_1 & \begin{pmatrix} -1.73 & 0.00 & 0.06 \\ 0.00 & -5.11 & 0.00 \\ -0.20 & 0.00 & -1.76 \end{pmatrix} & \text{O}_2 & \begin{pmatrix} -3.80 & -0.08 & -1.94 \\ -0.11 & -1.55 & -0.01 \\ -1.97 & 0.00 & -3.61 \end{pmatrix} \\
 & [-1.67 & -1.82 & -5.11] & & [-5.66 & -1.77 & -1.53]
 \end{array}$$

TABLE II: Calculated Born effective charge tensors (e) for the four inequivalent atoms of TAB.I. The eigenvalues of the symmetric part of the tensor are mentioned in the brackets.

The calculated electronic dielectric tensor is slightly anisotropic with values of 11.3, 13.1 and 10.8 along the x, y and z directions respectively. These values are larger than in the usual ABO_3 compounds (we obtain an average of 11.7 instead of about 6.0 for $CaTiO_3$ [13] or $BaTiO_3$ [17]) but coherent with the small band gap. This value of ϵ^∞ does not differ strongly from that previously reported in the ideal cubic structure (11.25 [17]), which contrasts with what is reported for orthorhombic $CaTiO_3$, where the ϵ^∞ decreases when non-polar distortions are frozen in the structure.

C. Phonons

The irreducible representation of the orthorhombic $Pnma$ $CaMnO_3$ at Γ point is: $7A_g \oplus 5B_{1g} \oplus 7B_{2g} \oplus 5B_{3g} \oplus 10B_{1u} \oplus 8B_{2u} \oplus 10B_{3u} \oplus 8A_u$. Over this decomposition, 3 modes are acoustic (B_{1u}, B_{2u}, B_{3u}), 8 are silent (symmetry A_u), 24 are Raman (R) active (symmetries A_g, B_{1g}, B_{2g} and B_{3g}) and the last 25 modes are Infrared (IR) active (symmetries B_{1u}, B_{2u} and B_{3u}). According to the structure defined in TAB.I, the IR B_{3u} modes are polarized along the x direction, B_{2u} along y direction and B_{1u} along z direction. The eight A_u silent modes not reported in the tables, are calculated at the frequencies 123, 140, 179, 220, 313, 392, 438 and 466 cm^{-1} .

1. Raman active modes

In TAB.III we report our calculated frequency of the Raman active modes. These frequencies are compared with experimental and shell model results from ref.[14]. Experimentally, the main observed modes are the ones with symmetry A_g . 10 A_g modes were measured at 150, 160, 184, 243, 278, 322, 382, 438, 487 and 615 cm^{-1} instead of 7 modes expected from group theory. The frequency at 615 cm^{-1} was unambiguously assigned to impurity and the modes at 382 and 438 cm^{-1} were kept aside since their frequencies differ strongly with the shell model. Below 200 cm^{-1} the assignment was also ambiguous since two modes are calculated at 154 and 200 cm^{-1} but three are observed in the spectra. From our calculation, the A_g modes at 250, 275 and 314 cm^{-1} could be assigned to the experimental ones at 243, 278 and 322 cm^{-1} respectively with a better frequency than the shell model. For the low frequency the assignment could be with better agreement than the shell model if we assign

the calculated modes at 152 and 167 cm^{-1} to the experimental ones at 150 and 160 cm^{-1} respectively instead of the modes measured at 160 and 184 cm^{-1} . For the high frequency A_g modes, we can assign the experimental mode at 438 cm^{-1} to the calculated one at 450 cm^{-1} instead of shell model assignment to the experimental mode at 487 cm^{-1} . Here, ambiguity could not be deleted since the experimental mode could be also attributed with the same error to our calculated A_g mode at 504 cm^{-1} .

The experimental mode at 179 cm^{-1} assigned as B_{1g} in Ref.[14] is in good agreement with our calculation (189 cm^{-1}). For the two experimental modes assigned to B_{3g} symmetry, we calculated the good frequency for the first one (320 cm^{-1}), but the second is bad estimated (469 cm^{-1} instead of 564 cm^{-1}). Since the assignment between B_{1g} and B_{3g} modes is ambiguous this experimental mode could be also associated to the B_{1g} mode calculated at 488 cm^{-1} or the even to the one calculated at 595 cm^{-1} with a better agreement.

If we follow the assignment of Ref.[14], the B_{2g} modes are less well calculated, since two B_{2g} are measured at 258 and 465 cm^{-1} and should be attributed to the calculated modes at 180 and 425 cm^{-1} according Ref.[14]. α and β are the cartesian directions (x, y or z), However, the third B_{2g} in our calculation is obtained at 227 cm^{-1} which could correspond with better agreement to the experimental frequency of 258 cm^{-1} . Moreover, the agreement with the second experimental B_{2g} mode at 465 cm^{-1} could be really increased if we make the assignment to the calculated one at exactly 465 cm^{-1} .

2. IR active modes

Table IV summarizes the calculated IR frequencies of the TO modes. No IR measurement of orthorhombic CaMnO_3 single crystal was found to compare with our results. An IR spectra is reported in Ref.[16] but it was done on a polycrystalline and no symmetry attribution is reported for the 15 observed frequencies which makes the comparison difficult considering the high number of modes. The only remark that could be done is at high frequency. The three highest frequencies are measured in Ref.[16] at 533, 580 and 628 cm^{-1} , which deviate strongly with our results where the maximum frequency of IR modes is calculated at 504 cm^{-1} . This could be related to the approximations of our calculations (LDA) or to a coupling between modes at the experimental level (for exemple the highest measured frequency could be recover as being the exact sum between the mode measured at 305 cm^{-1} and 323 cm^{-1}).

Symmetry	Calc.	Exp.	Calc.	Exp.
	This Work	Ref.[14]	Ref.[14]	Ref.[14]
A_g	152	150	154	160
A_g	167	160	200	184
B_{2g}	172	-	148	-
B_{2g}	180	-	232	258
B_{1g}	189	179	178	179
B_{3g}	203	-	290	-
B_{2g}	227	258	292	
B_{1g}	241	-	281	-
A_g	250	243	242	243
A_g	275	278	299	278
A_g	314	322	345	322
B_{3g}	320	320	304	320
B_{1g}	330	-	354	
B_{2g}	372	-	366	-
B_{2g}	425	-	453	465
B_{3g}	434	-	459	-
A_g	450	438	467	487
B_{2g}	465	465	485	
B_{3g}	469	-	541	564
B_{1g}	488	-	536	-
A_g	504	487	555	-
B_{1g}	595	564	743	-
B_{2g}	655	-	749	-
B_{3g}	674	-	754	-

TABLE III: Comparison of the calculated and experimental frequencies (cm^{-1}) of the Raman modes of orthorhombic CaMnO_3 . The first column represents the symmetry attribution of each mode, the second column corresponds to the calculated frequency in the framework of this paper, the third column is the experimental mode assignment with respect to our calculations and in the fourth and fifth columns are reported the calculated and experimental attribution respectively of Ref.[14].

Symmetry	Freq.	\bar{Z}^*	ε_0^m
B_{3u}	101	15.95	238.4
B_{1u}	147	10.74	35.09
B_{1u}	150	13.63	65.37
B_{3u}	153	13.63	4.06
B_{2u}	155	3.97	0.7
B_{2u}	179	2.03	11.4
B_{2u}	208	5.6	37.67
B_{1u}	215	14.27	5.8
B_{3u}	216	5.61	1.5
B_{3u}	234	3.10	3.9
B_{2u}	251	5.06	3.8
B_{3u}	287	4.6	1.8
B_{1u}	290	3.40	0.04
B_{2u}	324	0.59	0.37
B_{1u}	326	2.70	0.78
B_{3u}	340	2.59	0.13
B_{1u}	345	1.40	0.51
B_{1u}	381	2.36	1.8
B_{1u}	414	6.18	0.00
B_{3u}	423	0.06	0.25
B_{2u}	437	1.92	0.26
B_{3u}	469	1.89	1.07
B_{2u}	488	4.22	1.04
B_{3u}	495	4.14	0.09
B_{1u}	504	1.4	0.65

TABLE IV: Calculated frequencies of the 25 IR modes. The second column represent the mode effective charges (e) and the third column shows the corresponding contribution to the static dielectric constant along the polarization direction of the mode ($B_{1u} \rightarrow \varepsilon_0^{zz}, B_{2u} \rightarrow \varepsilon_0^{yy}, B_{3u} \rightarrow \varepsilon_0^{xx}$).

In addition we report the mode effective charges of each mode and the corresponding contribution to the dielectric constant in TAB.IV. The total static dielectric tensor could be calculated as following:

$$\epsilon_0^{\alpha\beta} = \epsilon_{\alpha\beta}^{\infty} + \sum_m \epsilon_{0,m}^{\alpha\beta}$$

where α and β are the cartesian directions (x, y or z), ϵ^{∞} is the electronic dielectric tensor and $\epsilon_{0,m}$ is the contribution to the dielectric constant by an individual phonon mode m and is computed from the following relation:

$$\epsilon_{0,m}^{\alpha\beta} = \frac{4\pi}{\Omega} \frac{S_m^{\alpha\beta}}{\omega_m^2}$$

where Ω is the volume of the cell, $S_m^{\alpha\beta}$ and ω_m are respectively the oscillator strength and the frequency of the mode m. The results show that only some modes contribute to the static dielectric constant. In the x direction, the static dielectric constant is mainly due to only one mode (B_{3u} mode at 101cm^{-1}), which is due to its high mode effective charge and low frequency. Its contribution to ϵ_0 is of about 238 while the total value is $\epsilon_0^{xx}=262$. In the other directions, the contributions come from few modes and is spread over two or three modes. The total static dielectric constant are calculated to be 68 along the y direction (ϵ_0^{yy}) and 120 along the z direction (ϵ_0^{zz}).

IV. CONCLUSION

The electronic structure and lattice dynamics of orthorhombic CaMnO_3 were studied from the first principle using first-principles methods. The shape of the cell and atomic positions obtained at the experimental volume are in good agreement with experimental datas, only the b axis is slightly overestimated. The band gap, Born effective charges and electronical dielectric tensor are obtained with the same amplitude than the ones reported in previous first-principle calculations for the ideal cubic structure. The Raman active phonons are compared with experimental frequencies and a good agreement is observed for the most modes but by modifying slightly the assignment made with previous shell model simulations. IR modes were also reported as well as their mode effective charges and their contribution to the static dielectric tensor.

The Born effective charges are calculated as being anomalous, with high values with respect to their nominal values of the ideal ionic configuration. These anomalous BECT

was also expected to be a condition on the possibility to obtain unstable polar distortions and ferroelectricity in ABO_3 structures. It is an indication of the propensity to polarize the compound or to make it ferroelectric. This indication could be confirmed from vibrational properties, since a mode with low frequency and high mode effective charge (*i.e.* highly polarizable) is observed in the x direction of the orthorhombic structure, which could play the role of a ferroelectric soft mode. However, in the case of orthorhombic $CaMnO_3$ no polar distortion is observed and it could be related to the competition between AFD and ferroelectric distortions which make $CaMnO_3$ non-polar like in $CaTiO_3$ or $SrTiO_3$.

V. ACKNOWLEDGEMENT

This work was supported by the European STREP MaCoMuFi, the VolkswagenStiftung and the European FAME-NoE.

-
- [1] C. Martin, A.Maignan, M. Hervieu and B. Raveau, Phys. Rev. B **60**, 12191 (1999)
 - [2] N.N Loshkareva, L.V Nomerovannaya, E.V Mostovshchikova, A.A. Makhnev, Yu. P. Sukhorukov, N.I. Solin T.I Arbuzova, S.V. Naumov and N.V. Kostromitina, A.M. Balbashov and L.N Rybina, Phys. Rev. B **70**, 224406 (2004)
 - [3] K. R. Poeppelmeir, M.E Leonowicz, J.C Scanlon, J.M Longo and Y.B Yelon, Journal of Solid State Chemistry, **45**, 71 (1982)
 - [4] S.F Matar, Progress in Solid State Chemistry, **31**, 239 (2003)
 - [5] J.H.Jung, K.H. Kim, D.J. Eom, T.W. Noh, E.J. Choi, Jaejun Yu, Y.S. Kwon and Y. Chung Phys. Rev. B **55**, 15489 (1997)
 - [6] F Freyria Fava, Ph D' Arco, R Orlando and R Dovesi, J. Phys. Condens. Matter, **9**, 489 (1997)
 - [7] M.Nicastro and C.H. Patterson, Phys. Rev. B **65**,205111 (2002)
 - [8] X. Gonze, J.-M. Beuken, R. Caracas, F. Detraux, M. Fuchs, G.-M. Rignanese, L. Sindic, M. Verstraete, G. Zerah, F. Jollet, M. Torrent, A. Roy, M. Mikami, Ph. Ghosez, J.-Y. Raty, D.C. Allan. Computational Materials Science **25**, 478-492 (2002).
 - [9] X. Gonze and C. Lee, Phys. Rev. B **55**, 10355 (1997).
 - [10] C. Hartwigsen, S. Goedecker and Hutter Phys. Rev.B **58** 3641 (1998)

- [11] J.L. Cohn, M. Peterca, J.J Neumeier, Journal of Applied Physics, **97**, 034102 (2003)
- [12] J.L. Cohn, M. Peterca, J.J Neumeier, Phys. Rev. B, **70**, 214433 (2004)
- [13] E. Cockayne and B. P. Burton, Phys. Rev. B **62**, 3735 (2000).
- [14] M.V. Abrashev *et al* Phys. Rev. B **65** 184301 (2002)
- [15] J. H. Jung and al., Phys. Rev. B **55**, 15489 (1997).
- [16] I.Fedorov, J.Lorenzana,P.Dore,G.De Marzi,P.Maselli, P.Calvani, S.W. Cheong, S. Koval and R. Migoni, Phys. Rev. B **60**, 11875 (1999)
- [17] A. Filippetti and N. A. Hill, Phys. Rev. B **65**, 195120 (2002).

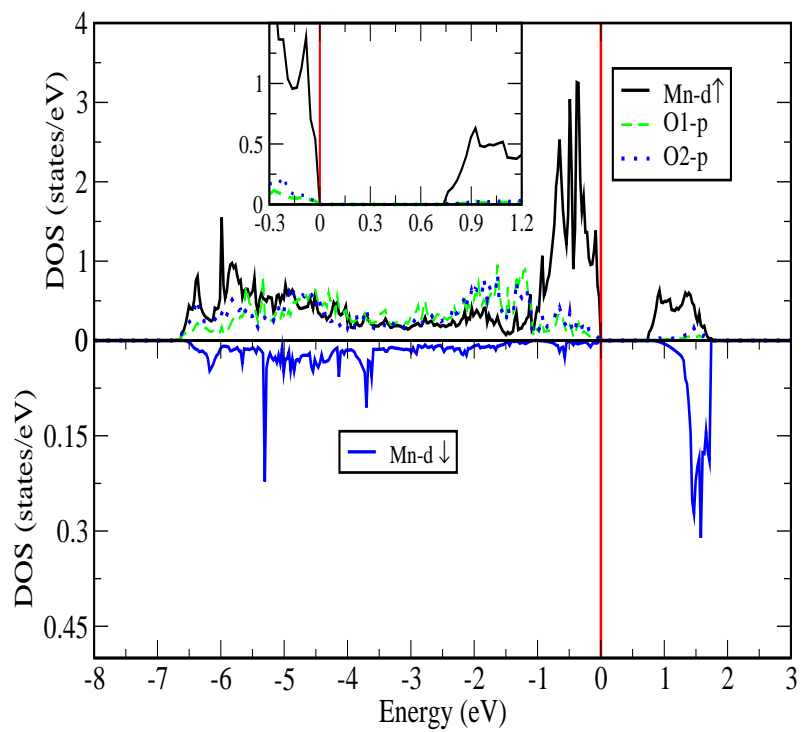


FIG. 1: Calculated DOS of orthorhombic CaMnO_3